JACS
JOURNAL OF THE AMERICAN CHEMICAL SOCIETY

Communication

pubs.acs.org/JACS

Complex Archimedean Tiling Self-Assembled from DNA Nanostructures

Fei Zhang, Yan Liu,* and Hao Yan*

Department of Chemistry and Biochemistry and the Biodesign Institute, Arizona State University, Tempe, Arizona 85287, United States

Supporting Information

ABSTRACT: Archimedean tilings are periodic polygonal tessellations that are created by placing regular polygons edge-to-edge around a vertex to fill the plane. Here we show that three- and four-arm DNA junction tiles with specifically designed arm lengths and intertile sticky-end interactions can be used to form sophisticated two-dimensional (2D) and three-dimensional (3D) tessellation patterns. We demonstrate two different complex Archimedean patterns, ($3^3.4^2$) and ($3^2.4.3.4$), and the formation of 2D lattices, 3D tubes, and sealed polygon-shaped pockets from the tessellations. The successful growth of hybrid DNA tile motif arrays suggests that it maybe possible to generate 2D quasi-crystals from DNA building blocks.

Archimedean tilings, which are periodic tessellations created by placing regular polygons edge-to-edge around a vertex, were first classified by Johannes Kepler in 1619[1] and are still of great interest today because of the unique and interesting properties of the resulting patterns. For example, Archimedean tilings can be used to generate photonic crystals, which are periodic optical nanostructures that affect the propagation of electromagnetic waves in much the same way that semiconductors affect electrons.[2] Another report describes a specific Archimedean tiling, ($3^3.4^2$), that forms a "wetting layer" between periodic and quasi-crystalline phases in a binary colloidal system.[3] Recent progress in structural DNA nanotechnology reveals that tiling can also be achieved using DNA nanostructures.

Synthetic DNA molecules are powerful and effective materials for the construction of addressable two-dimensional (2D) and three-dimensional (3D) nanostructures[4] and have demonstrated their potential use in nanoelectronic, biosensing, and computational applications.[5] Multiarm junctions in particular have been widely used for the assembly of various 2D and 3D structures by programming unique intertile sticky-end interactions to create more complex higher-order structures.[6] However, previous reports of their assembly are mostly based on repeating patterns of uniform geometric building blocks (regular tiling), which can be treated as a special case of Archimedean tiling with homogeneous vertices, tiles, and edges.

In this work, we utilized combinations of precisely designed three- and four-arm DNA junction tiles to generate rationally designed, sophisticated 2D and 3D tessellation nanostructures. In contrast to regular tilings, semiregular Archimedean tilings are composed of more than one type of regular polygon[7] and thus require at least two unique building blocks. We demonstrate that two Archimedean tilings, ($3^2.4.3.4$) and ($3^3.4^2$) (Figure 1a,b), can be created through the self-assembly of three- and four-arm DNA junction tiles. Our results show that both tilings assemble into 2D lattice arrays with dimensions on the micrometer scale. Changing the design of the junctions (lengths of the arms and complementarity of the sticky ends) and tuning the annealing conditions enables the formation of tubes and pockets displaying the same Archimedean pattern. The successful formation of these hybrid DNA junction patterns establishes a foundation for the construction of more complex higher-order DNA nanostructures or even DNA quasi-crystals.

The first step in the design process is to select desirable lengths for the arms of the DNA motifs to make them spatially compatible and able to facilitate connections between building blocks. Here there are two important factors to consider: the geometry/dimensions of the desired Archimedean tiling and the 3D helical structure of double-stranded (ds) DNA. For semiregular Archimedean patterns formed from equilateral triangle and square motifs (Figure 1a,b), the two polygons have the same edge length. The two motifs can be represented by three- and four-arm junctions and transformed into Cairo pentagonal and Prismatic pentagonal tilings by connecting the junctions. The geometric constraints of the tiling parameters require an arm length ratio (four-arm:three-arm) of $3^{1/2}$:1 (=1.732). This ratio allows the tiles to be assembled in such a way that the arms do not overlap or have gaps between them, ensuring that any compression/stretching or bending of the DNA double helices is minimized. It is also important to consider that B-form dsDNAs are 3D molecules that exhibit 10.5 base pairs (bp) per helical turn in solution. For quasi-2D and 2D structures, the distance between the crossovers in adjacent tile arms is restricted to even (all tiles face-up) or odd (alternating face-up and face-down) numbers of half-turns, respectively. Adhering to these restrictions avoids deviations of the self-assembled structures from the desired quasi-2D and 2D patterns and minimizes over- or undertwisting of the DNA strands.

With these two considerations in mind, three different combinations of arm lengths (defined in terms of the number of helical turns) corresponding to the four-arm and three-arm junction tiles were evaluated: 4.5:2.5 (=1.80), 3.5:2.0 (=1.75) and 4.0:2.25 (=1.78). The arm length ratio thus ranged from 1.75 to 1.80. The corresponding tiling patterns are shown in Figure

Received: April 10, 2013
Published: May 7, 2013

dx.doi.org/10.1021/ja4035957 | J. Am. Chem. Soc. 2013, 135, 7458−7461

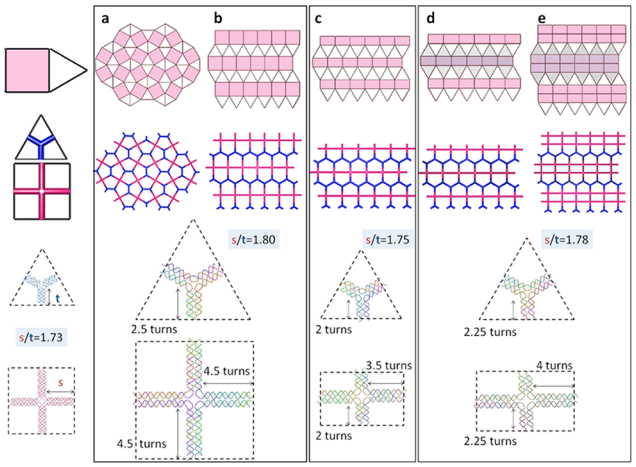

Figure 1. Designing the length of the arms in DNA junction tiles to create different Archimedean tiling patterns. (a) Archimedean tiling pattern ($3^2.4.3.4$) and the corresponding transformed Cairo pentagonal tiling (upper panels), which can be represented by three-arm and four-arm DNA junction motif tiles with arm lengths of 2.5 and 4.5 turns, respectively, giving an arm length ratio of 1:1.80 (lower panels). (b) Archimedean tiling pattern ($3^3.4^2$) and the corresponding transformed Prismatic pentagonal tiling (upper panels), which can be represented by three-arm and four-arm junction motifs with the same arm lengths as in (a) (lower panels). (c) Shortened Archimedean tiling ($3^3.4^2$) and transformed shortened Prismatic pentagonal tiling (upper panels), in which the multiarm junction motifs have arm lengths of 2 and 3.5 turns, respectively (1:1.75 ratio) (lower panels). It should be noted that the length of the arms in the four-arm junction tile is shorter in the vertical direction (2 turns). (d) Shortened Archimedean tiling with a corrugated design and shortened Prismatic pentagonal tiling with neighboring layers of unit cells facing in opposite directions (gray indicates face-down) (upper panels). Here the multiarm junction motifs have arm lengths of 2.25 and 4 turns, respectively (1:1.78 ratio) (lower panels). (e) The more complex 3-isogonal tiling formed when an extra layer of rectangular tiles is included, and the corresponding transformed 2-uniform tiling (upper panels). The same multiarm junction motifs as in (d) are used to create this pattern (lower panels).

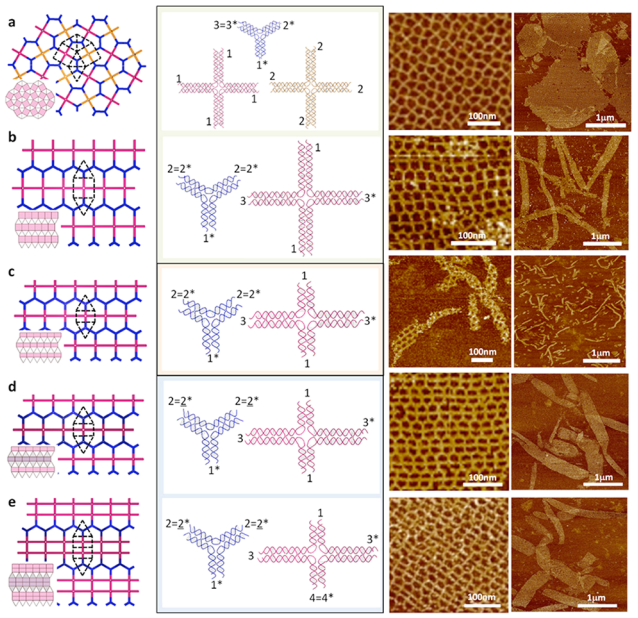

Figure 2. Sticky-end matching rules and corresponding AFM images for the five Archimedean tiling designs: (a) Cairo pentagonal tiling corresponding to the Archimedean tiling ($3^2.4.3.4$); (b) Prismatic pentagonal tiling corresponding to the Archimedean tiling ($3^3.4^2$); (c) shortened Prismatic pentagonal tiling; (d) shortened Prismatic pentagonal tiling with corrugated design; (e) 2-uniform tiling with an extra layer of rectangular tiles and corrugated design. In each row from left to right, the first panel illustrates the unit cell, represented by dashed lines. The second panel depicts the sticky-end matching rules: sticky end *n* interacts with *n**, and underlined numbers represent tiles that are connected to other tiles facing in the opposite direction in the array (a half-turn between vertices in the DNA arms). The third and fourth panels are zoomed-in and zoomed-out AFM images, respectively, with the scale bars marked.

1a–e. These length ratios satisfy the structural requirements of DNA double helices to ensure that the edge-to-edge distances between the junction points in the assemblies are either whole- or half-helical turns and therefore that adjacent DNA tiles are either facing the same direction or opposite faces of the same 2D plane. In addition, these combinations of arm lengths are relatively close to the ideal geometric ratio of 1.732. Because of the inherent flexibility and soft-materials properties of DNA, this small discrepancy can apparently be accommodated. We restricted the arm lengths (a maximum of nine full turns or 31 nm between the vertices) to maintain the rigidity of the DNA.

In the nonisotropic tiling patterns shown in Figure 1b–e, the four sides of the squares do not have to be of equal length; the squares can be replaced by rectangles, or multiple layers of rectangles can be introduced without interrupting the overall periodic lattice growth. The only geometric requirement is that the side of the rectangle motif that is in contact with the equilateral triangle motif must have the same length as the side of the triangle. Meanwhile, the sides that are in contact with other squares or rectangles can be any length that satisfies the requirements imposed by the properties of the DNA double helices and crossover patterns.

The second step in the design process is to identify the matching rules corresponding to the desired patterns and to encode the specific interunit interactions within the sticky ends of the tiles. Archimedean tiling has translational periodicity based on "unit cells". We can determine the unit cell within each pattern and use the multiarm DNA junction motifs to construct these unit cells. By considering the symmetry of the unit cells, we can specify the unique sticky ends and minimize the number of different DNA building blocks required. For example, the unit cell of the pattern shown in Figure 2b (also called Prismatic pentagonal tiling with Prismatic-pentagon-shaped cavities) is an elongated hexagon that can be constructed from two three-arm motifs and one four-arm motif. Here we designed a single three-arm motif (instead of two) that contains one arm (1*) that interacts with arm 1 from the four-arm motif and two arms that are self-complementary (2 and 2*). Meanwhile, the four-arm motif contains two opposite arms (1) that can be connected with arm 1* of the three-arm motif and two opposite arms that are self-complementary (3 and 3*). We anticipated that mixing these two tiles in a 2:1 molar ratio would result in the self-assembly of the units into the pattern depicted in Figure 2b.

However, symmetry within the DNA motifs can increase the possibility of mismatched interactions. It is important to carefully balance the simplicity of the building blocks with the ability to form a unique pattern. For example, when we attempted to construct the tiling pattern shown in Figure 2a, also called Cairo pentagonal tiling, from one four-arm motif (instead of two) with the same sticky ends (1 = 2 and 1* = 2*), we did not obtain the expected pattern, and only small mismatched pieces were

dx.doi.org/10.1021/ja4035957 | J. Am. Chem. Soc. 2013, 135, 7458–7461

observed. It is likely that the symmetry of the four-arm tile motif reduced the probability of forming a unique structure. [See the schematics in Figure S1 in the Supporting Information (SI).] Thus, designing building blocks with precisely encoded sticky-ends is essential for the successful formation of the desired pattern. In this case, we had to use two unique four-arm tiles and one unique three-arm tile to realize the design. By mixing these three unique tiles in a 1:1:4 molar ratio, we facilitated the self-assembly of the unit motifs into the expected pattern shown in Figure 2a.

The final step in the design process is to assign sequences to the ssDNA comprising each structural motif and the corresponding sticky ends. First, we found that asymmetric sequences are required for the arms, even for cases when the sticky-ends are the same. For example, in the Cairo pentagonal tiling (Figure 2a), each four-arm tile has four identical sticky-ends but still requires four different sequences for the branches to avoid aggregation at the individual tile level (see Figure S10b). This is likely because the arms used here are much longer than the ones described previously,[6b,c,e,8] so the strands with repeating sequences have a greater chance to be linked to other tiles. Second, the sequences of the sticky ends should be distinct to avoid mismatches between building blocks. It is also important to note that GC-rich sequences in the sticky-end designs should be avoided to prevent undesired oligomerization of the individual tile motifs (Figure S10c,d). In the work reported here, we utilized 4 bp sticky ends throughout. The total of $4^4 = 256$ possibilities provides an adequate sequence space for the selection of unique interunit complementarity.

Figure 2a demonstrates the formation of the Cairo pentagonal tiling corresponding to the Archimedean pattern ($3^2.4.3.4$) in which the three-arm and four-arm building blocks are combined in a 4:1:1 ratio. Atomic force microscopy (AFM) characterization of the products confirmed that the tiles self-assembled into micrometer-sized 2D arrays. The AFM images also revealed that the 2D arrays often exhibited curved edges, indicating that they were not perfectly planar in solution before deposition onto mica (see the additional images in Figure S2a). This curvature is likely an intrinsic consequence of the design, as the tiles are all facing the same direction and thus any curvature in the individual tiles may be accumulated in the 2D array. However, the relatively large size of the arrays (with dimensions of several micrometers) indicates that the curvature of the unit tiles, if any, was small (<1° per tile).

Figure 2b illustrates the formation of the Prismatic pentagonal tiling corresponding to the Archimedean pattern ($3^3.4^2$). Its two building blocks have the same arm lengths as those in the Cairo pentagonal tiling (Figure 2a) but different sticky-end sequences as determined by its own matching rules. Similarly, these tiles all face in the same direction in the array. When mixed in a molar ratio of 2:1, they self-assembled into large 2D sheets that curled up into tubes with diameters of 80−250 nm (see the diameter distribution in Figure S3c and the additional AFM images in Figure S3d).

Tube formation from DNA tile arrays has been discussed previously.[9] This process is thermodynamically allowed as long as the enthalpy gained from DNA hybridization at the edges of the tile arrays is sufficient to compensate for the decrease in entropy and the energetic cost of bending the helices within the tile arrays. On the basis of the designed connection pattern, there are four possible ways to fold the 2D array into a tube (see the schematics in Figure S3a). We carefully analyzed AFM images of 88 tubes and found that in ∼57% of them the long axis was parallel to the connections between the four-arm junction tiles (Figure S3e), while ∼43% of the tubes adopted a spiral arrangement with the long axis of the tube at an angle of <45° with respect to the connections between the four-arm junction tiles. There was no evidence of the formation of structures in which the axis of the tube was perpendicular to the connections between the four-arm junctions tiles, nor were there any tubes that adopted angles of >45° with respect to the intertile connections.

These observations can be explained in terms of the anisotropic growth dynamics of the tile arrays. The growth rate parallel to the direction of the four-arm tile−tile association is expected to be much faster than that in the perpendicular direction. This is the case because the rate of growth in the array per building block is faster in the parallel direction than in the perpendicular direction, as the four-arm junction tiles are larger in size and require a single pair of sticky-end interactions per tile to secure the subsequent layer of tiles. In contrast, the growth rate in the perpendicular direction per unit tile is smaller, not only because each three-arm tile is shorter but also because growth in that direction requires at least two successful pairs of sticky-end connections per tile to secure the next layer of tiles. This growth dynamics causes the anisotropic elongation of the tile array that we observed. Given enough time during the annealing process, the 2D tile arrays will reach a point at which it is more difficult and energetically unfavorable for the tiles along the edges to encounter complementary tiles in solution than it is for them to interact with other edges of the array and form tubes. It is also possible for ring structures to form during the nucleation step; these structures can serve as templates that can be elongated from both ends, resulting in the formation of tubes. Shorter tubes may also be connected end-to-end during the last stage of the annealing process to form longer tubes.

Figure 2c shows a shortened Prismatic pentagonal tiling that uses the same matching rules as shown in Figure 2b but with shorter arms in both of the component tiles (less than integer numbers of half-turns in each arm). Therefore, the tiles all face in the same direction but the anisotropy in the dimensions is higher. The building blocks were found to connect and curl into tubes with relatively small diameters of ∼43 nm (Figure S4e). The narrow tubes form within 2 h and grow longer with extended annealing times (see the SI for detailed experimental methods and Figure S4b). This observation supports a nucleation and growth mechanism. The tube-folding direction is similar to that in the Prismatic pentagonal design and can be explained in the same way as discussed above (Figure S4).

Figure 2d shows another shortened Prismatic pentagonal tiling, but this one has a corrugated design in which the lengths of the arms are adjusted according to Figure 1d to ensure that the neighboring layers of unit cells alternately face up and down. This design balances the natural curvature within the building blocks and leads to formation of large 2D arrays. Interestingly, wide tubes (see the additional AFM images in Figure S5a,b) with diameters (or half-perimeters) of 100−400 nm (Figure S5c) were observed. It appears that the formation of tubes cannot be prevented with a corrugated design. This result indicates that the 2D arrays are flexible enough that bending them incurs a smaller energetic penalty than the energy released from base pairing.

As shown in Figure 2e, we further modified the four-arm building block compared with the design in Figure 2d so that only one of the sticky ends was self-complementary (4 = 4*). When the three- and four-arm tiles were mixed in a 1:1 ratio, they self-assembled into a complex 2D tiling. This was also a

dx.doi.org/10.1021/ja4035957 | J. Am. Chem. Soc. 2013, 135, 7458−7461

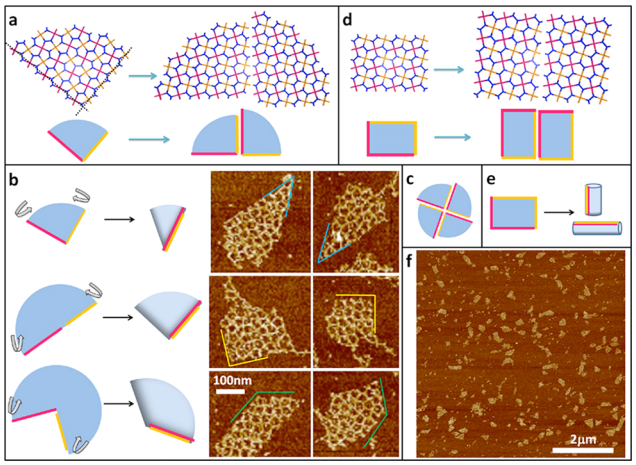

Figure 3. Possible mechanisms of the formation of two-layer pocketlike structures. (a) In the Cairo pentagonal tiling, two edges are arranged at a 90° angle and are complementary to each other. (b) Three possible folding interactions in which interedge angles of 90°, 180°, and 270° lead to folded angles of 45°, 90°, and 135°, respectively. The corresponding structures are shown in the AFM images on the right. (c) On the basis of (a), four sets of matching edge interactions point to a center. (d) Two parallel edges match each other to bring two smaller pieces together to form a larger piece. (e) Parallel edges allow a 2D array to fold into a tube. (f) AFM image of the sample obtained from a 0.5:0.5:4 ratio of building blocks (the ideal ratio for the large 2D array is 1:1:4).

corrugated design with neighboring layers of unit cells alternately facing opposite directions. The arrays formed from this design also curled into tubes with diameters of 100−450 nm (Figure S6c), similar to those in Figure 2d. The cavities in this pattern exhibited both rectangular and Prismatic pentagonal shapes.

We further investigated the parameters that influence the formation of large patterns, including the molar ratio of the building blocks, the annealing program, and concentration. For the shortened Prismatic pentagonal tiling with a corrugated design that was assembled using a short annealing time (2 h instead of 12 h), a low concentration of building blocks (0.2 μM instead of 0.6 μM), and a deviation from the desired stoichiometric ratio (1:0, 0:1, 1:1, or 1:1.9 instead of 1:2), only small fragments were observed (Figures S7 and S8). However, for the Cairo pentagonal tiling when the ratio of building blocks was varied from the designed value of 4:1:1 (Figure S9) to 8:1:1 or 2:1:1, we observed the formation of small, two-layer structures with sharp edges and dimensions of 200−500 nm. These pocketlike structures were also observed in the background of the large 2D array samples when a 4:1:1 ratio was used (Figure S2b), possibly as a result of the imperfect stoichiometric ratio. The pockets were likely to adopt the observed shapes with certain preferred angles. Figure 3 illustrates the possible mechanisms of folding when two complementary edges with angles of 90°, 180°, and 270° come together to form pocketlike structures; after deposition on 2D substrates for AFM imaging, they form two-layer structures with sharp angles of 45°, 90°, and 135°, respectively.

In 2008, researchers determined that the intermediate between a crystal and a quasi-crystal is a $(3^3.4^2)$ Archimedean-like tiling structure, which was observed in a colloidal monolayer interacting with a quasi-crystalline substrate.[10] Later, a link between Archimedean tilings and quasi-crystals was established when the self-assembly of binary nanoparticles resulted in the formation of quasi-crystalline superlattices with a $(3^3.4^2)$ Archimedean structure interface between the quasi-crystalline and crystalline phases.[3] It is foreseeable that the successful hybridization of DNA motifs to form Archimedean tiling structures will further increase the complexity of DNA nanostructures and provide the ability to form quasi-crystals based on DNA tiling. Furthermore, DNA-directed assembly of quasi-crystalline arrays may produce unique nanostructures with novel properties through functionalization of the DNA tile motifs with other nanomaterials.

■ ASSOCIATED CONTENT

Supporting Information

Experimental details and additional data. This material is available free of charge via the Internet at http://pubs.acs.org.

■ AUTHOR INFORMATION

Corresponding Author

yan_liu@asu.edu; hao.yan@asu.edu

Notes

The authors declare no competing financial interest.

■ ACKNOWLEDGMENTS

This work was supported by grants from the National Science Foundation (1104373), the Office of Naval Research (N000140911118), and the Army Research Office (ARO) (W911NF-11-1-0137) to H.Y. and Y.L. and an ARO MURI Award (W911NF-12-1-0420) to H.Y. H.Y. was also supported by the Presidential Strategic Initiative Fund of Arizona State University. We thank Dr. Jeanette Nangreave for proofreading the manuscript.

■ REFERENCES

(1) Grünbaum, B.; Shephard, G. C. *Tilings and Patterns*; Freeman: New York, 1987.

(2) David, S.; Chelnokov, A.; Lourtioz, J. M. *IEEE J. Quantum Electron.* **2001**, *37*, 1427.

(3) Talapin, D. V.; Shevchenko, E. V.; Bodnarchuk, M. I.; Ye, X.; Chen, J.; Murray, C. B. *Nature* **2009**, *461*, 964.

(4) (a) Seeman, N. C. *J. Theor. Biol.* **1982**, *99*, 237. (b) Rothemund, P. W. K. *Nature* **2006**, *440*, 297. (c) Winfree, E.; Liu, F. R.; Wenzler, L. A.; Seeman, N. C. *Nature* **1998**, *394*, 539.

(5) (a) Seeman, N. C. *Nature* **2003**, *421*, 427. (b) Gothelf, K. V.; LaBean, T. H. *Org. Biomol. Chem.* **2005**, *3*, 4023. (c) Voigt, N. V.; Tørring, T.; Rotaru, A.; Jacobsen, M. F.; Ravnsbæk, J. B.; Subramani, R.; Mamdouh, W.; Kjems, J.; Mokhir, A.; Besenbacher, F.; Gothelf, K. V. *Nat. Nanotechnol.* **2010**, *5*, 200. (d) Deng, Z. T.; Samanta, A.; Nangreave, J.; Yan, H.; Liu, Y. *J. Am. Chem. Soc.* **2012**, *134*, 17424.

(6) (a) Yan, H.; Park, S. H.; Finkelstein, G.; Reif, J. H.; LaBean, T. H. *Science* **2003**, *301*, 1882. (b) He, Y.; Chen, Y.; Liu, H. P.; Ribbe, A. E.; Mao, C. D. *J. Am. Chem. Soc.* **2005**, *127*, 12202. (c) He, Y.; Tian, Y.; Ribbe, A. E.; Mao, C. D. *J. Am. Chem. Soc.* **2006**, *128*, 15978. (d) He, Y.; Tian, Y.; Chen, Y.; Ribbe, A. E.; Mao, C. D. *Chem. Commun.* **2007**, 165. (e) Zhang, C.; Su, M.; He, Y.; Zhao, X.; Fang, P.-a.; Ribbe, A. E.; Jiang, W.; Mao, C. *Proc. Natl. Acad. Sci. U.S.A.* **2008**, *105*, 10665.

(7) Chavey, D. *Comput. Math. Appl.* **1989**, *17*, 147.

(8) He, Y.; Ye, T.; Su, M.; Zhang, C.; Ribbe, A. E.; Jiang, W.; Mao, C. *Nature* **2008**, *452*, 198.

(9) (a) Ke, Y. G.; Liu, Y.; Zhang, J. P.; Yan, H. *J. Am. Chem. Soc.* **2006**, *128*, 4414. (b) Maune, H. T.; Han, S.-p.; Barish, R. D.; Bockrath, M.; Goddard, W. A., III; Rothemund, P. W. K.; Winfree, E. *Nat. Nanotechnol.* **2010**, *5*, 61. (c) Mitchell, J. C.; Harris, J. R.; Malo, J.; Bath, J.; Turberfield, A. J. *J. Am. Chem. Soc.* **2004**, *126*, 16342.

(10) Mikhael, J.; Roth, J.; Helden, L.; Bechinger, C. *Nature* **2008**, *454*, 501.